11566–11576 *Nucleic Acids Research, 2020, Vol. 48, No. 20* *Published online 14 October 2020*
doi: 10.1093/nar/gkaa862

Inhibition of *Plasmodium falciparum* Lysyl-tRNA synthetase via an anaplastic lymphoma kinase inhibitor

Jintong Zhou[1], Zhenghui Huang[2], Li Zheng[1], Zhoufei Hei[1], Zhiyong Wang[1], Biao Yu[1,3], Lubin Jiang[2,*], Jing Wang[1,3,*] and Pengfei Fang[1,3,*]

[1]State Key Laboratory of Bioorganic and Natural Products Chemistry, Center for Excellence in Molecular Synthesis, Shanghai Institute of Organic Chemistry, University of Chinese Academy of Sciences, Chinese Academy of Sciences, 345 Lingling Road, Shanghai 200032, China, [2]Unit of Human Parasite Molecular and Cell Biology, Key Laboratory of Molecular Virology and Immunology, Institut Pasteur of Shanghai, University of Chinese Academy of Sciences, Chinese Academy of Sciences, 320 Yueyang Road, Shanghai 200031, China and [3]School of Chemistry and Materials Science, Hangzhou Institute for Advanced Study, University of Chinese Academy of Sciences, 1 Sub-lane Xiangshan, Hangzhou 310024, China

Received August 24, 2020; Revised September 17, 2020; Editorial Decision September 17, 2020; Accepted September 23, 2020

ABSTRACT

Aminoacyl-tRNA synthetases are attractive targets for the development of antibacterial, antifungal, antiparasitic agents and for the treatment of other human diseases. Lysyl-tRNA synthetase (LysRS) from this family has been validated as a promising target for the development of antimalarial drugs. Here, we developed a high-throughput compatible assay and screened 1215 bioactive compounds to identify *Plasmodium falciparum* cytoplasmic LysRS (*Pf*LysRS) inhibitor. ASP3026, an anaplastic lymphoma kinase inhibitor that was used in clinical trials for the treatment of B-cell lymphoma and solid tumors, was identified as a novel *Pf*LysRS inhibitor. ASP3026 suppresses the enzymatic activity of *Pf*LysRS at nanomolar potency, which is >380-fold more effective than inhibition of the human counterpart. In addition, the compound suppressed blood-stage *P. falciparum* growth. To understand the molecular mechanism of inhibition by ASP3026, we further solved the cocrystal structure of *Pf*LysRS-ASP3026 at a resolution of 2.49 Å, providing clues for further optimization of the compound. Finally, primary structure-activity relationship analyses indicated that the inhibition of *Pf*LysRS by ASP3026 is highly structure specific. This work not only provides a new chemical scaffold with good druggability for antimalarial development but also highlights the potential for repurposing kinase-inhibiting drugs to tRNA synthetase inhibitors to treat human diseases.

INTRODUCTION

Malaria is a parasitic infection caused by single-celled parasites of the genus *Plasmodium*, including *P. falciparum*, *P. knowlesi*, *P. vivax*, *P. malariae* and *P. ovale*. Among them, *P. falciparum* is the most prevalent malaria parasite in Africa, accounting for 99.7% of estimated malaria cases in 2018 (1). Significant progress has been made in the last decade in reducing malaria incidence and mortality globally (2). However, half of the world's population still lives at risk from this disease. Approximately 3.1 billion people live in malaria-endemic areas (tropical and subtropical). In 2018, an estimated 228 million cases of malaria occurred worldwide, killing ∼405 000 people, mostly children (1). Importantly, drug-resistant *P. falciparum* and *P. vivax* parasites have evolved in the Greater Mekong Subregion, the island of Papua and South America, respectively (3). The growing resistance to artemisinin-based combination therapies, the first-line treatment of *P. falciparum*, threatens the sustainability of recent gains in malaria control and the long-term prospects for eliminating malaria. Drugs with new chemical scaffolds are of high priority for the development of antimalarials.

Aminoacyl-tRNA synthetases (aaRSs) are essential enzymes for all cellular life, playing a central role in the translation of the genetic code (4,5). These enzymes catalyze the transfer of amino acids to their cognate tRNAs as building blocks for protein/peptide biosynthesis. AaRSs are proven

*To whom correspondences should be addressed. Tel: +86 21 5492 5308; Email: fangpengfei@sioc.ac.cn
Correspondence may also be addressed to Jing Wang. Tel: +86 21 5492 5106; Email: jwang@sioc.ac.cn
Correspondence may also be addressed to Lubin Jiang. Tel: +86 21 5492 3072; Email: lbjiang@ips.ac.cn

to be attractive targets for developing antibacterial, antifungal, antiparasitic agents and for treating other human diseases (6–11). *P. falciparum* has 37 aaRS genes, which encodes 36 aaRS enzymes (12). Of the 36 aaRSs, 16 are exclusively present in cytoplasm, 15 are exclusive to apicoplast, and four are shared by cytoplasm and apicoplast (13). These enzymes are all indispensable for parasite growth and survival.

In fact, there has been a long history of fighting malaria by inhibiting the activity of aaRSs. The herb *Dichroa febrifuga* was used to treat malaria more frequently in traditional Chinese medicine than the *Artemisia annua*, the extract of which contains artemisinin (14). The active ingredient of *D. febrifuga* is febrifugine, which has antimalarial activity (15) and is a specific proly-tRNA synthetase (ProRS) inhibitor (16). In addition, the threonyl-tRNA synthetase (ThrRS) inhibitor borrelidin was also reported to have potent antimalarial activity (17,18). Borrelidin suppresses drug-sensitive FCR3 strain and drug resistant K1 strain of *P. falciparum* (17), and protects mice from lethal malaria infection (19). These examples demonstrate that aaRS inhibitors exhibit great potential to be developed as antimalarial drugs.

It was recently discovered that a potent lysyl-tRNA synthetase (LysRS) inhibitor cladosporin is active against blood- and liver-stage *P. falciparum* (20). This chemical shows high species specificity against *P. falciparum* cytoplasmic LysRS (*Pf*LysRS) with a 1000-fold lower IC_{50} compared to other eukaryotic LysRSs including human LysRS (20), and inhibits *Pf*LysRS with an IC_{50} of approximately 4 nM (21). This species specificity is not only related to the active site binding residues, but is also connected to the backbone plasticity of the *Pf*LysRS (22,23). These important findings provide very strong validations of LysRS as a drug target for malaria. However, the poor oral bioavailability and high metabolic instability prevent cladosporin from becoming an antimalarial drug. Analogs and more ATP-competitive inhibitors of *Pf*LysRS are being actively developed (21,24–26). In particular, new chemical scaffolds with good druggability are of great value.

Here, we developed a high-throughput compatible assay and screened 1215 bioactive compounds to identify *Pf*LysRS inhibitors. Surprisingly, ASP3026, which was used in clinical trials for the treatment of B-cell lymphoma and solid tumors, was discovered to be a potent *Pf*LysRS inhibitor. The safety, pharmacokinetic profile, and antitumor activity of ASP3026 have been previously assessed through an open-label, multicenter, first-in-human phase I study (27). ASP3026 exhibits very good oral absorption and ideal metabolic stability. It is well tolerated and has therapeutic activity in patients with crizotinib-resistant ALK-positive advanced tumors (27). It is also reported to be a novel inhibitor of erythrocyte cell membrane scrambling following energy depletion and oxidative stress (28). In this study, we show that ASP3026 suppresses the enzymatic activity of *Pf*LysRS at nanomolar concentrations. It inhibits blood-stage *P. falciparum* 3D7 growth with an IC_{50} of 5.61 $\pm$ 0.26 μM. We further reveal the molecular mechanism for the inhibition of *Pf*LysRS by ASP3026 by solving the cocrystal structure of *Pf*LysRS-ASP3026 at a resolution of 2.49 Å. In addition, primary structure-activity relationship analyses show that the inhibition of *Pf*LysRS by ASP3026 is highly structure specific. Together, we report here the discovery of a new aaRS inhibitor, which provides a promising chemical scaffold for antimalarial development and highlights the potential of repurposing kinase-inhibiting drugs as aaRS inhibitors to treat human diseases.

MATERIALS AND METHODS

Protein expression

*Pf*LysRS (77–583) wabs constructed in the vector pET20b with a C-terminal 6× His tag. The protein was expressed in BL21 (DE3) strain with 0.2 mM isopropyl-beta-D-thiogalactopyranoside (IPTG) for 20 h at 16°C. The cell pellet (from 4 to 8 l) was lysed in the wash buffer containing 500 mM NaCl, 20 mM Tris–HCl pH 8.0, and 15 mM imidazole. Then, the supernatant of the lysate was loaded onto a Ni-HiTrap column and washed with wash buffer. The protein was eluted with the elution buffer containing 500 mM NaCl, 20 mM Tris–HCl pH 8.0, and 250 mM imidazole. Then the protein was concentrated and further purified by gel filtration, using a Superdex 200 Increase size exclusion column (GE Healthcare) with running buffer containing 20 mM HEPES pH 7.5, and 150 mM NaCl (Supplementary Figure S1). The peak fractions were then concentrated for thermal shift assays, surface plasmon resonance assays, ATP hydrolysis assays or crystallization experiments. *Hs*LysRS (70–581) was constructed in the vector pET20b with a C-terminal 6× His tag, and purified similarly. The protein concentrations used in all the experiments were determined by the Bradford method (29).

Thermal shift assay

For compound screening, *Pf*LysRS protein was prepared at 1 μM concentration in a buffer containing 20 mM Tris–HCl pH 8.0, 200 mM NaCl, 100 μM L-lysine, 100 μM AMP and 1× SYPRO Orange dye (Sigma). Aliquots (99 μl) of the mixture were added into each well of a 96-well PCR plate. Then 1 μl of compounds (10 mM stock) or DMSO control were added to the PCR plate. After complete mixing, the final solutions were heated from 25 to 70°C at a rate of 0.015°C/s, and the fluorescence signals were monitored by QuantStudio 3 (Applied Biosystems by Thermo Fisher Scientific).

To validate the primary hits, *Pf*LysRS protein was prepared at 10 μM concentration in a buffer containing 20 mM Tris–HCl pH 8.0, 200 mM NaCl, 500 μM L-lysine, and 200 μM compound. Aliquots (18 μl) were added to a 96-well PCR plate and incubated at ambient temperature for 10 min. SYPRO Orange dye (Sigma) was diluted in the assay buffer containing 20 mM Tris–HCl pH 8.0 and 200 mM NaCl to a 40× concentration, and 2 μl of the 40× dye solution was added to the PCR plate to bring the final assay volume to 20 μl. After complete mixing, the final solutions were heated from 25 to 90°C at a rate of 0.015°C/s, and fluorescence signals were monitored by QuantStudio 3 (Applied Biosystems by Thermo Fisher Scientific).

The dissociation constants (K_D) between *Pf*LysRS and inhibitors can be estimated from the increase in the protein's mid-melting temperature (T_m) induced by inhibitors

through a previously established method (22,30). Briefly, a nonlinear least squares fitting algorithm was used to fit the fluorescence curve using the following expression: $y(T) = yu + \frac{yf-yu}{1+\exp\{-\Delta Hu/R[\frac{1}{T}-\frac{1}{Tm}]+\Delta Cpu/R[\ln(\frac{T}{Tm})+\frac{Tm}{T}-1]\}}$, where $y(T)$ is the fluorescence unfolding data; R is the gas constant; and the five parameters, T_m, ΔHu, ΔCpu, yf, and yu, are obtained from curve fitting. ΔHu is the protein unfolding enthalpy. ΔCpu is the heat capacity change for protein unfolding. yf and yu are the pretransitional and posttransitional fluorescence intensity levels, respectively. Then, the dissociation constant at Tm (K_D^{Tm}) is calculated using the following expression: $K_D^{Tm} = \frac{[L]_{Tm}}{\exp\{-\Delta Hu^{T0}/R[\frac{1}{Tm}-\frac{1}{T0}]+\Delta Cpu^{T0}/R[\ln(\frac{Tm}{T0})+\frac{T0}{Tm}-1]\}}$, where $[L]_{Tm}$ is the free ligand concentration at Tm, which can be estimated by $[L]_{Total}$. T0 is the midpoint for the protein unfolding transition in the absence of ligand. ΔHu^{T0} is the enthalpy of protein unfolding in the absence of ligand. ΔCpu^{T0} is the heat capacity change for protein unfolding in the absence of ligand. Finally the K_D at 25°C/298 K can be estimated by the expression: $K_D = \frac{K_D^{Tm}}{\exp\{62760/R[\frac{1}{298}-\frac{1}{Tm}]\}}$, where 62 760 ($J \cdot mol^{-1}$) is an estimation of the ligand binding enthalpy (30).

ATP hydrolysis assay

ATP hydrolysis activity of LysRS was assayed using the Malachite Green Phosphate assay system (Sigma-Aldrich catalog no. MAK307) in a BIOFIL 96-well tissue culture plate. The assay was performed in an 80-μl volume containing 100 nM *Pf*LysRS or 500 nM *Hs*LysRS in 40 mM HEPES pH 7.5, 1 mM DTT, 8 mM $MgCl_2$, 500 μM L-lysine, 100 μM ATP, and indicated concentrations of the inhibitor. Assay without the inhibitor was used as a negative control (NC), and assay without L-lysine was used as a positive control (PC). The reagent mixture was vortexed at 1000 rpm for one min, followed by an incubation at 30°C for 6 h. The enzymatic activity was terminated by the addition of 20 μl of Working Reagent from the kit according to the manufacturer's instructions. Then, the mixture was vortexed at 1000 rpm for one min and left at room temperature for 30 min. The absorbance (OD 612 nm) was measured on the Magellan plate reader (Tecan). The % inhibition was calculated by (NC-absorbance) × 100/(NC-PC). Because pyrophosphate could increase the absorbance by itself (Supplementary Figure S2A), no pyrophosphatase was used in the assay systems. Withdrawal of L-lysine or replacement of L-lysine by noncognate amino acids, such as L-asparagine and L-cysteine, failed to increase the absorbance confirming that the increase in absorbance was tightly related to the L-lysine activation activity of LysRS (Supplementary Figure S2B).

Surface plasmon resonance (SPR) assay

*Pf*LysRS was chemically immobilized on a Biacore CM5 sensorchip (immobilization level ∼10691 resonance unit, RU) at pH 5.5 according to the immobilization kit (GE Healthcare). *Pf*LysRS (33 nM) was captured for 90 s at a flow of 30 $\mu l \cdot min^{-1}$. Affinity between *Pf*LysRS and ASP3026 was measured by SPR on a Biacore T200 (GE Healthcare) at 25°C with a running buffer (0.02 M phosphate buffer pH 7.4, 2.7 mM KCl, 0.137 M NaCl, 1 mM L-lysine, and 0.05% Surfactant P20). ASP3026 dilutions were made to yield (dissolved in running buffer) at concentrations of 1000, 500, 250, 125 and 62.5 nM (association time: 90 s, dissociation time: 120 s, flow: 30 $\mu l \cdot min^{-1}$). To study the ATP competitive nature of ASP3026, 1 mM ATP or 4 μM cladosporin analog 3-(cyclohexylmethyl)-6,8-dihydroxy-1H-isochromen-1-one was included in the running buffer. Kinetic evaluation of the interaction between LysRS and ASP3026 was performed by global fitting of the data to a 1:1 interaction model using Biacore Evaluation Software 3.1 (GE Healthcare).

Mammalian protein translation assay

The effects of compounds on the mammalian protein translation system were assayed in a rabbit reticulocyte lysate according to the manufacturer's instructions (Promega) with the exceptions that no extra amino acid mix was added and 0.005 $mg \cdot ml^{-1}$ of firefly luciferase mRNA was used in the assays.

In vitro Plasmodium growth assay

Parasites were cultured in human O+ erythrocytes according to standard procedures. To prepare the >80% ring stage parasites, asynchronous cultures of parasites were pretreated with 5% sorbitol, and *P. falciparum* strain 3D7 at the mid-ring stage (6–10 h post-invasion) was used to test antimalarial effects in 96-well plates. Parasites were incubated in a 96-well plate with compound containing 1% parasitemia and 2% hematocrit for a total volume of 200 μl. The compounds were diluted from the maximum concentration of 10 μM with a 2-fold gradient dilution for total 11 points. A relevant DMSO concentration was used as a negative control (NC), and cultured erythrocytes without *Plasmodium* served as a positive control (PC). The parasites were allowed to grow for 72 h at 37°C with 5% CO_2, 5% O_2, and 90% N_2. After 72 h, 100 μl of lysis buffer (0.12 $mg \cdot ml^{-1}$ Saponin, 0.12% Triton X-100, 30 mM Tris–HCl pH 8.0, and 7.5 mM EDTA) with 5× SYBR Green I (Invitrogen; supplied in 10 000× concentration) was added to each well of the plate. The plates were then incubated for 2 h in the dark prior to reading the fluorescence signal at 485 nm excitation and 535 nm emission. The % inhibition was calculated by (NC-fluorescence) × 100/(NC-PC). To evaluate the effects of compound on the morphology of parasites, ring stage parasites was treated with compound at a final concentration of 25 μM containing 1% parasitemia and 2% hematocrit for a total volume of 10 ml, and DMSO was used as control. Giemsa stain blood smears were made at 0, 24, 48 and 72 h after treatment. Parasites morphology was observed using a microscope.

Protein crystallization

All crystallizations were performed using the sitting drop method. *Pf*LysRS protein (30 $mg \cdot ml^{-1}$) was premixed with 1 mM of ASP3026 and 1 mM of L-lysine at 4°C and was

Table 1. Data collection and refinement statistics

	*Pf*LysRS-ASP3026
PDB code	7BT5
Data collection	
Space group	$P2_12_12$
Cell dimensions	
a, *b*, *c* (Å)	97.75, 166.40, 70.92
α, β, γ (°)	90.00, 90.00, 90.00
Resolution (Å)	50.00–2.49 (2.58–2.49)
R_{sym} or R_{merge} (%)	8.9 (68.4)
$I/\sigma(I)$	12.7 (2.7)
Completeness (%)	99.9 (100.0)
Redundancy	7.3 (7.5)
Refinement	
Resolution (Å)	50.00–2.49 (2.58–2.49)
Total reflections	41114
R_{work}/R_{free} (%)	21.4/24.0
No. atoms	
Protein	7652
Ligand	102
Solvent	133
B-factors	
Protein	68.25
Ligand	64.04
Solvent	57.26
R.m.s. deviations	
Bond length (Å)	0.005
Bond angle (°)	1.070
Ramachandran plot	
Most favored (%)	96.85
Additional allowed (%)	3.15

Statistics for the highest-resolution shell are shown in parentheses.

crystallized by mixing 0.4 μl of protein solution with 0.4 μl of precipitant solution, containing 0.1 M MES pH 6.0, and 15% PEG4000. After incubation at 18°C for 3–7 days, crystals were flash-frozen in liquid nitrogen for data collection with the cryo-solution containing 0.08 MES pH 6.0, 12% PEG4000, 20% glycerol and 1 mM ASP3026.

Structure determination

The *Pf*LysRS-ASP3026 complex crystal diffraction datasets were obtained from beamline 17U1 at Shanghai Synchrotron Radiation Facility (SSRF) (31). All datasets were processed with Xia2 (32). The structures were solved by molecular replacement using the *Pf*LysRS structure (PDB code: 4YCV) with the program Molrep (33). Iterative model building and refinement were performed using Coot and Phenix (34,35). Data collection and refinement statistics are given in Table 1.

RESULTS

High-throughput compatible thermal shift assay for developing *Pf*LysRS inhibitors

Previous studies have shown that the thermal stability of *Pf*LysRS could be largely increased when the protein is bound to small molecule inhibitors such as the natural product cladosporin or its analogs (22,25,36). Based on this information, we optimized a high-throughput compatible assay to screen for strong *Pf*LysRS inhibitory binders (Supplementary Figure S3). Because the synergistic binding of inhibitors with substrate amino acids and adenosine was previously found in *Pf*LysRS and ProRS (10,22), we performed the screening in the presence of 100 μM L-lysine, and 100 μM adenosine. Dimethyl sulfoxide (DMSO) and cladosporin analog 3-(cyclohexylmethyl)-6,8-dihydroxy-1H-isochromen-1-one were used as negative and positive controls, respectively (Supplementary Figure S3B) (37).

We screened a library of 1215 bioactive compounds from Selleck Chemicals (Figure 1A, Supplementary Table S1). A total of 14 plates were used for this assay (Figure 1B). As indicated from the positive and negative control scatterplots, the entire screen demonstrated an excellent Z' factor (0.77 ± 0.07) (Figure 1B). Finally, eighteen compounds showed an apparent increase in the mid-melting temperature (T_m) of the *Pf*LysRS of >4°C. These compounds were subjected to enzymatic assays.

ASP3026 is a novel *Pf*LysRS inhibitor

ASP3026, a recently developed anaplastic lymphoma kinase (ALK) inhibitor (38), is among the lead hits (Figure 1A). ASP3026 contains an (N^2,N^4-diphenyl-1,3,5-triazine-2,4-diamine, Ph-Az-Ph) core structure, an isopropylsulfonyl- substituent on the first phenyl moiety, and 2-methoxy-4-(4-methylpiperazinyl)piperidinyl- substituents on the second phenyl moiety (Figure 2A). The ASP3026-mediated increase in the thermal stability of *Pf*LysRS is very well repeated (Figure 2B, Supplementary Figure S4). The compound significantly increased the Tm of *Pf*LysRS by 10.0°C without the presence of the amino acid L-lysine and by 8.0°C in the presence of L-lysine (Figure 2B, C). This finding indicated that the binding of ASP3026 to *Pf*LysRS was independent of L-lysine. This characteristic is distinct to cladosporin, which binds to *Pf*LysRS via a mechanism that is strongly dependent on the presence of L-lysine (22). The K_D of *Pf*LysRS-ASP3026 complex was estimated to be approximately 238 nM based on the ΔT_m of 10.0°C in the presence of L-lysine (see Materials and Methods). We also performed surface plasmon resonance (SPR) experiments and calculated the K_D kinetically using the ratio of the dissociation rate constant (k_{off}) to the association rate constant (k_{on}) (Figure 2D). Sensorgram analysis for the interactions of ASP3026 with immobilized *Pf*LysRS resulted in k_{on} 2.64E04 ± 4.50E02 $M^{-1}\cdot s^{-1}$ and k_{off} 6.30E-03±4.20E-05 s^{-1} with K_D 239 nM. To further confirm the inhibition activity of ASP3026 against *Pf*LysRS, we performed an ATP-hydrolysis assay, which is the first step of the aminoacylation reaction catalyzed by aaRSs. ASP3026 demonstrated potent inhibition of *Pf*LysRS with an IC_{50} of 657 ± 195 nM (Figure 2E, Supplementary Figure S5), which is at the same order of magnitude of the K_D of the *Pf*LysRS–ASP3026 complex. These results indicate that ASP3026 is a novel inhibitor of *Pf*LysRS.

ASP3026 inhibited *Plasmodium* growth but not mammalian protein translation

To determine the inhibitory effect of ASP3026 on *Plasmodium* growth, *P. falciparum* 3D7 parasites were synchronized to the ring stage and treated with ASP3026, and parasite maturation was monitored over 72 h. The parasites

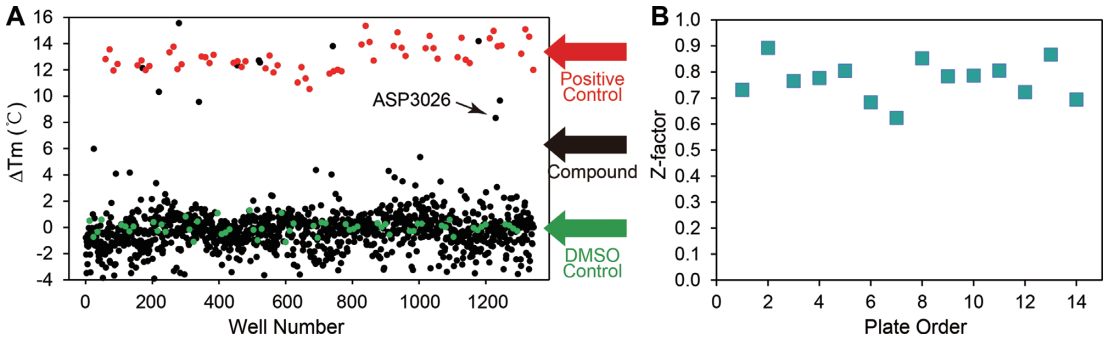

Figure 1. High-throughput screening for *Pf*LysRS inhibitors based on the thermal shift assay. (**A**) Scatterplot from the bioactive library (black dot), positive control (3-(cyclohexylmethyl)-6,8-dihydroxy-1*H*-isochromen-1-one, red dot), and negative control (DMSO, green dot). (**B**) Stable *Z*'-factors of the 14 plates in the experiment.

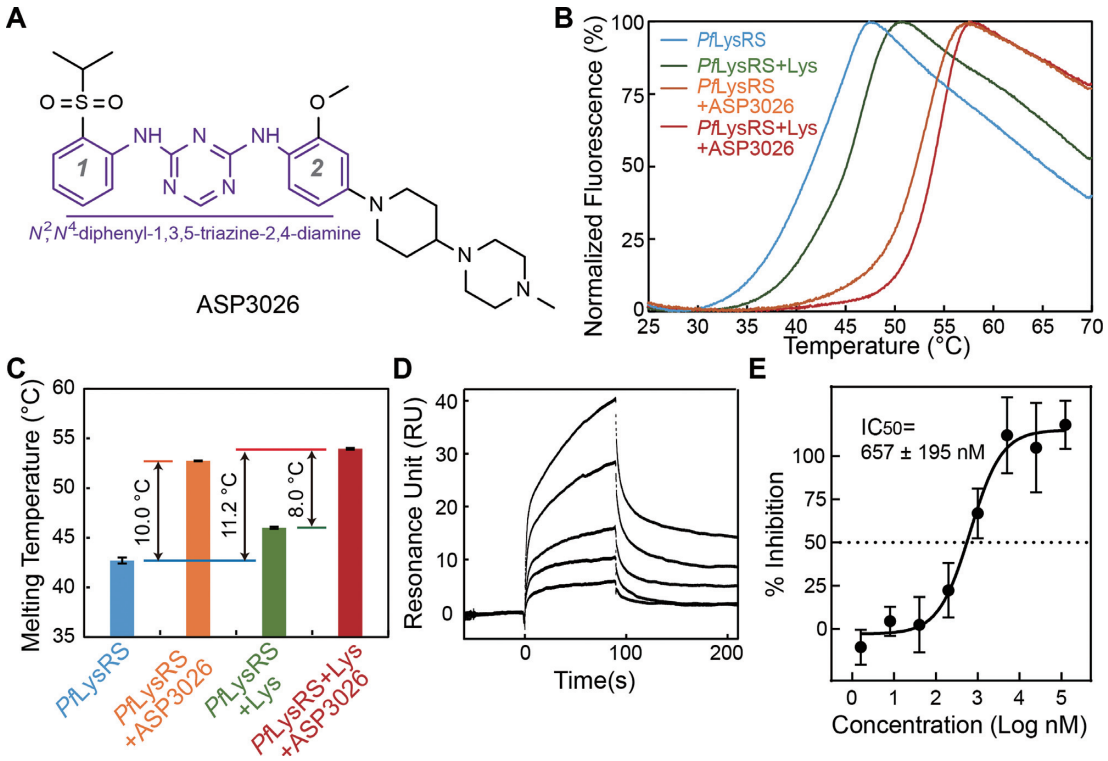

Figure 2. ASP3026 is a novel *Pf*LysRS inhibitor. (**A**) The chemical structure of compound ASP3026. The core structure N^2,N^4-diphenyl-1,3,5-triazine-2,4-diamine (Ph-Az-Ph) is highlighted in purple. (**B**) Thermal melting profile of *Pf*LysRS in the presence of L-lysine (Lys) and/or compound ASP3026. The fluorescent signals were normalized to minimum (0%) and maximum (100%). Each curve is an average of four measurements. (**C**) Diagram of the Tms of *Pf*LysRS in the presence of L-lysine (Lys) and/or compound ASP3026. Error bars represent standard deviations (SD) of four technical repeats. (**D**) Surface plasmon resonance (SPR) sensorgrams for the interaction of ASP3026 with immobilized *Pf*LysRS. The five curves are generated from 1000, 500, 250, 125 and 62.5 nM ASP3026 from top to bottom. (**E**) The potency of ASP3026 against *Pf*LysRS is measured using the ATP hydrolysis assay. Error bars represent SD of three technical repeats.

treated with solvent control could reproduce asexually, and the transition from trophozoite to schizont was observed in the Giemsa-stained blood smears (39). However, parasites treated with ASP3026 stopped growing completely until they eventually died (Figure 3A). We further evaluated the inhibitory potency of ASP3026 on *P. falciparum* strain 3D7 in the red stage. In this experiment, parasite growth is determined by using SYBR Green I, a dye with marked fluorescence enhancement upon contact with *Plasmodium* DNA (40). The IC_{50} was 5.61 ± 0.26 μM (Figure 3B), confirming the antimalarial activity of ASP3026.

To study the species selectivity of ASP3026, we examined the inhibition of ATP-hydrolysis of *Hs*LysRs by ASP3026. As a result, no significant inhibition was observed at all assayed concentrations of ASP3026, and the IC_{50} is greater than 250 μM, which is over 380-fold less potent than the IC_{50} of the ATP hydrolysis activity of *Pf*LysRS (Figure 3C). Consistently, ASP3026 could not increase the thermal stability of *Hs*LysRS in the presence or absence of L-lysine (Figure 3D). Further, we used a rabbit reticulocyte lysate based *in vitro* protein translation assay to evaluate the inhibitory effect of ASP3026 on mammalian protein trans-

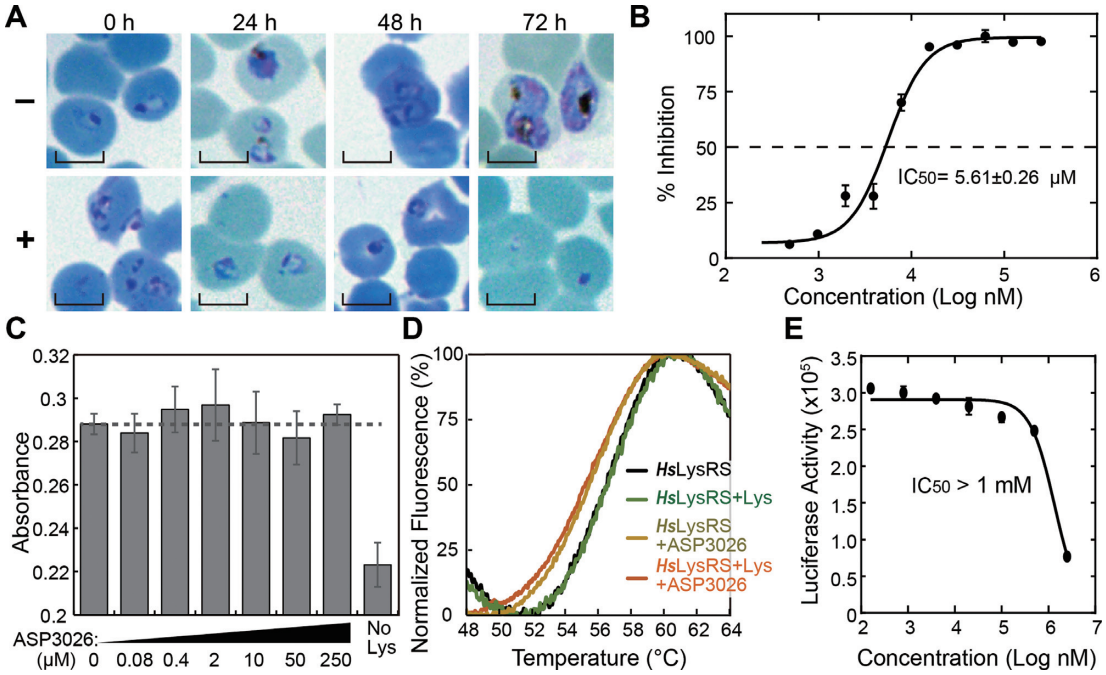

Figure 3. ASP3026 suppressed the growth of erythrocytic-stage parasites but not mammalian protein translation. (**A**) The specific time of action for ASP3026 in erythrocytic-stage parasites (strain 3D7) was determined by treating synchronized parasites and monitoring the cultures over a 72-h period. The morphology of untreated parasites (–) and parasites treated with 25 μM ASP3026 (+) were monitored by Giemsa-stained thin blood smears. Scale bars: 5 μm. (**B**) ASP3026 inhibits the growth of erythrocytic-stage parasites with an IC_{50} of 5.61 μM. Error bars represent SD of six biological repeats. (**C**) Up to 250 μM ASP3026 did not inhibit of human LysRS (*Hs*LysRS) in the ATP hydrolysis assay. L-lysine was withdrawn from the assay as a control (No Lys). Error bars represent SD of three technical repeats. (**D**) Thermal melting profile of *Hs*LysRS in the presence of L-lysine (Lys) and/or compound ASP3026. The fluorescent signals were normalized to minimum (0%) and maximum (100%). Each curve is an average of four measurements. (**E**) The potency of ASP3026 against the mammalian protein translation system. Error bars represent SD of three technical repeats.

lation. As a result, ASP3026 only suppressed the mammalian protein translation at a high concentration with an IC_{50} of greater than 1 mM (Figure 3E). Together, these results show that ASP3026 can effectively inhibit *Pf*LysRS activity and parasite growth but minimally suppresses mammalian LysRS, and these findings are consistent with previous research that ASP3026 is a largely nontoxic compound (27).

Crystal structure of *Pf*LysRS–ASP3026 complex

To understand how ASP3026 is recognized by *Pf*LysRS, we sought to determine the crystal structure of the *Pf*LysRS–ASP3026 complex. We cocrystallized the protein-inhibitor complex and solved the structure using the molecular replacement method. The structure was ultimately refined to a resolution of 2.49 Å (Table 1, Supplementary Figure S6). There are two *Pf*LysRS monomers forming a typical class II synthetase dimer within one asymmetric unit (ASU), and clear electron densities of ASP3026 are observed in each of the activity centers of the two monomers (Figure 4A, B). The Ph-Az-Ph core structure of ASP3026 occupied the adenine binding site (Figure 4C). The triazine moiety formed stacking interactions with the class II aaRS conserved Phe342 residue (Figure 4C and Supplementary Figure S7A). The sulfonyl moiety bound to the site that is normally bound by the ribose moiety of the substrate ATP (Figures 4C and Supplementary Figure S7B). The last methylpiperazine moiety extended out of the pocket (Figure 4C), and the electron density for this moiety is slightly weaker than the remainder of the compound (Figure 4B), suggesting that the methylpiperazine moiety is less important for the compound's potency in *Pf*LysRS inhibition. In total, 20 residues from *Pf*LysRS formed 235 atomic contacts with 32 nonhydrogen atoms of ASP3026 within 4.5 Å (Supplementary Table S2). These residues include Ala287, Arg330, Glu332, Gly330, Asp335, Thr337, His338, Asn339, Pro340, Phe342, Glu500, Val501, Leu502, Asn503, Gly554, Leu555, Gly556, Asp558, Arg559 and Ile570. Most of these interactions are hydrophobic interactions, and only the main chain atoms of Asn339 formed two hydrogen (H-) bonds with two nitrogen atoms of the azine and imine groups (Supplementary Table S2, Figure 4D). The structure indicated that ASP3026 competes with ATP for the *Pf*LysRS binding. Consistently, when we performed the SPR experiment in the presence of ATP, the sensorgram is significantly changed from that noted in the absence of ATP, and the binding kinetics can no longer be reliably calculated under this condition (Supplementary Figure S7C). Nonetheless, apparent decreases in the resonance units (RU) for all concentrations of ASP3026 are observed, which might be attributed to the competition between ATP and ASP3026. In addition, adding the cladosporin analog 3-(cyclohexylmethyl)-6,8-dihydroxy-1H-isochromen-1-one, which exhibits higher activity against *Pf*LysRS (25,37), completely suppressed the resonance (Supplementary Figure S7C), confirming that ASP3026 binds to the ATP pocket of *Pf*LysRS.

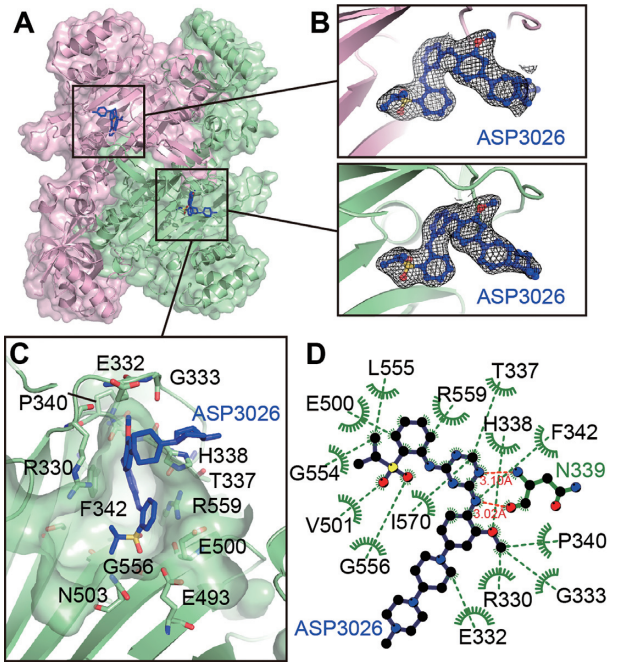

Figure 4. Recognition of ASP3026 by *Pf*LysRS. (**A**) Overview of *Pf*LysRS-ASP3026 structure determined at a resolution of 2.49 Å. A *Pf*LysRS dimer is shown in the cartoon and transparent surface. ASP3026 molecules are depicted as sticks. (**B**) The $2F_o - F_c$ electron densities maps (black meshes) of ASP3026 are contoured at 1.0 σ. (**C**) Zoom-in view of ASP3026 localization in the conserved ATP binding site of *Pf*LysRS. ASP3026 and residues within 4.5 Å are depicted as sticks. (**D**) Two-dimensional presentation of ASP3026 binding in *Pf*LysRS. ASP3026 and hydrogen-bonding residues are shown in stick representations, and other residues within 4.5 Å of ASP3026 are shown in green.

Interestingly, ASP3026 did not block the substrate L-lysine binding site in the *Pf*LysRS active center, and it is located 3.6 Å away from the oxygen atom of L-lysine (Supplementary Figure S7D). In addition, extending out of the ATP binding subsite, the 4-methylpiperazinyl-piperidinyl part of ASP3026 clashed with the C74C75 of modeled tRNA (Supplementary Figure S7E). Therefore, ASP3026 competes with ATP and tRNA but not L-lysine for *Pf*LysRS binding.

Conformational changes of *Pf*LysRS Induced by ASP3026

The complex structure of *Pf*LysRS-ASP3026 was largely consistent with the structure of *Pf*LysRS complexing with cladosporin and cladosporin analogs (22,36,37,41). The room-mean-square deviation (RMSD) between *Pf*LysRs-ASP3026 and *Pf*LysRs-cladosporin was 0.733 Å for 449 superimposed Cα atoms (36,41) (Figure 5A). However, the outer side of the active site cleft, including residues 410–460, showed a larger shift, which was up to 2 Å (Figure 5B). The *Pf*LysRS-ATP structure is not currently available. Superimposition of the human LysRS-ATP structure with the *Pf*LysRS-ASP3026 structure revealed an even greater conformational change (up to 5 Å shift) at this region (Figure 5C,D), which was significantly larger than the overall RMSD (0.833 Å) between human LysRS and *Pf*LysRS structures (Figure 5C). These comparisons recalled our previous discovery that the natural compound borrelidin induced a 14° and 10 Å-opening of the outer active site of ThrRS (18). These analyses suggest that class II aaRSs share some common flexibility of the active site pocket, which should be taken into account in future structure-based drug development.

Glu332 plays important roles in ATP and cladosporin recognition. It formed H-bond interactions with the amino group of ATP or the phenol group of cladosporin (36,41) (Supplementary Figure S8A,B). However, ASP3026 pushed the side chain of this residue to the outer direction by 57.5° and 3.3 Å (Figure 5E). In addition, the residue Glu500 held the phosphates of ATP through cobound metal ions or interacted with the methyltetrahydropyran moiety of cladosporin (36,41) (Supplementary Figure S8C,D). Its conformation was changed by the sulfonylphenyl moiety of ASP3026 with a rotation of 54.8° and a movement of 3.2 Å (Figure 5F). Finally, ASP3026 also triggered conformational changes to the residues Arg330 and His338, which are two other important residues for ATP recognition (Figure 5G). Therefore, ASP3026 induced more robust conformational changes than previously reported LysRS inhibitors.

In the thermal shift assay, we did not observe any synergistic effect between L-lysine and ASP3026 (Figure 2B,C). In our *Pf*LysRS–ASP3026 structure, the electron density for the substrate L-lysine is relatively weaker than the active site residues and ASP3026 (Supplementary Figure S9A). Bound L-lysine is slightly shallower than that in the *Pf*LysRS-cladosporin-L-lysine cocrystal structure (Supplementary Figure S9B) (36,41). This difference is possibly attributed to the smaller isopropyl group of ASP3026 than the methyltetrahydropyran moiety of cladosporin (Supplementary Figure S9B). This notion suggests that the synergistic effect of cladosporin and L-lysine is not only dependent on the co-occupation of the ATP and L-lysine pockets but also relies on the van der Waals interaction between the inhibitor and L-lysine. Therefore, a potential strategy to improve the potency of ASP3026 against *Pf*LysRS is to substitute the isopropylsulfonyl- moiety with a larger moiety, for example, a cyclohexyl- moiety (Supplementary Figure S9C). This substitution may mimic the van der Waals interaction between cladosporin and L-lysine and cause the new compound to synergistically bind with L-lysine to further increase the potency (Supplementary Figure S9D).

Structure-activity profile of ASP3026 substructure and analogs for *Pf*LysRS inhibition

We further tested the analogs and substructures of ASP3026 for binding with *Pf*LysRS using the thermal shift assay to explore the structure-activity relationship (Figure 6A,B). None of the substructural fragments **a**, **b**, **c**, and **bc** exhibited an effect on the thermal stability of *Pf*LysRS (Figure 6B), which is consistent with our observation that the major portion of ASP3026 formed interactions with *Pf*LysRS (Figure 4C, D) and that the potency of ASP3026 required the entire structure. Of the six tested analogs, NVP-TAE684 exhibits minimal change from ASP3026. The only difference between NVP-TAE684 and ASP3026 is that in NVP-TAE684, a phenylchloride substituted one azine in the Ph-Az-Ph core scaffold of ASP3026 (Figure 6A). Interestingly,

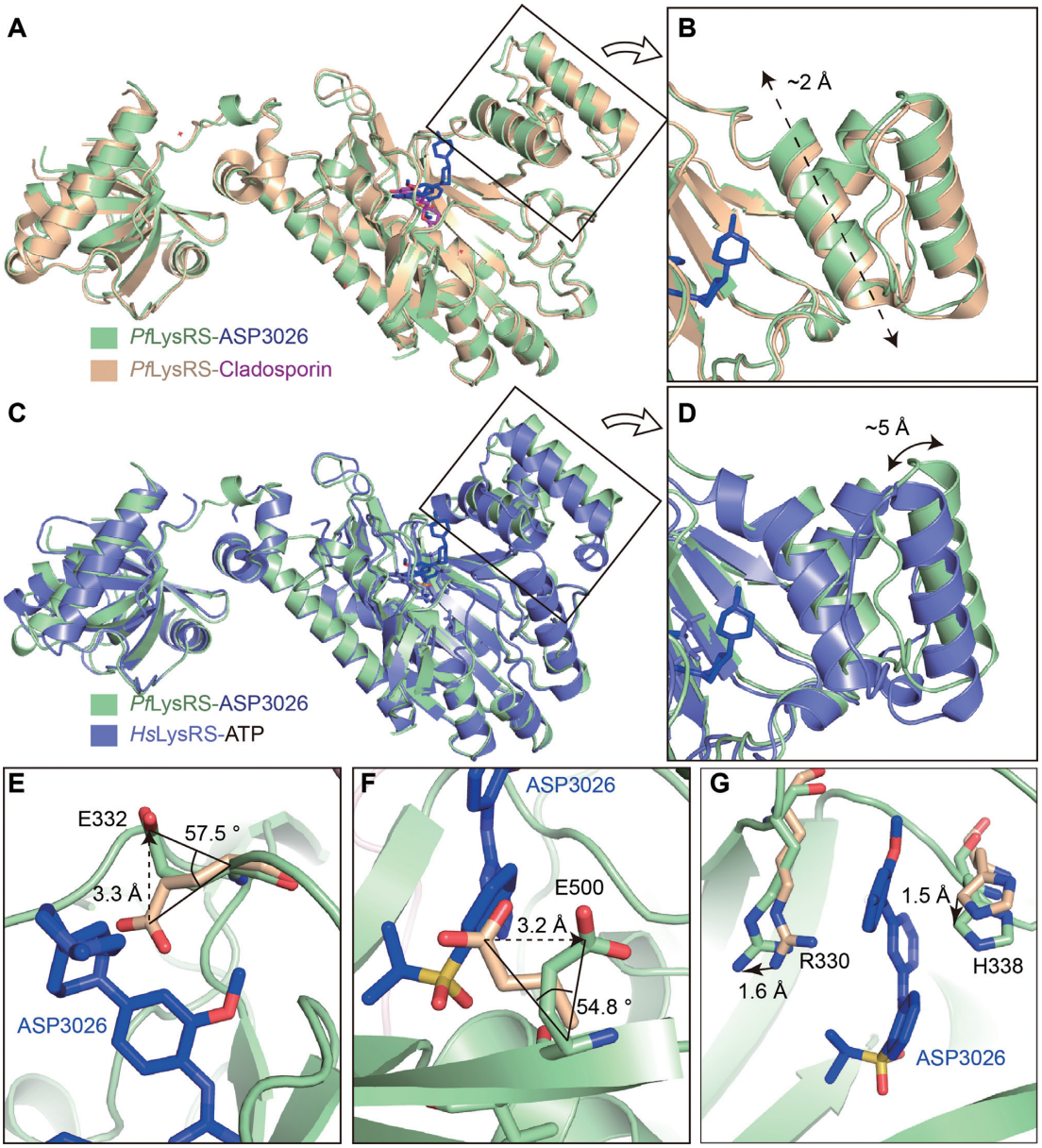

Figure 5. Conformational changes of *Pf*LysRS induced by ASP3026. (**A**) Superimposition of the structures of *Pf*LysRS–ASP3026 (this study) and *Pf*LysRS-cladosporin (PDB ID: 4PG3). ASP3026 and cladosporin are depicted as sticks. (**B**) The outer side of the active site cleft including residues 410–460 exhibited an up to 2 Å shift. (**C**) Superimposition of the structures of *Pf*LysRS-ASP3026 (this study) and *Hs*LysRS-ATP (PDB ID: 3BJU). ASP3026 and ATP are depicted as sticks. (**D**) The outer side of the active site cleft of *Pf*LysRS-ASP3026 structure exhibited greater conformational changes (up to 5 Å shift) when superimposed with the *Hs*LysRS-ATP structure. (**E**) ASP3026 pushed the side chain of residue Glu332 to the outer direction by 57.5° and 3.3 Å. ASP3026 and Glu332 are depicted as sticks. (**F**) The sulfonylphenyl moiety of ASP3026 changed the residue Glu500 conformation with a rotation of 54.8° and a movement of 3.2 Å. ASP3026 and Glu500 are depicted as sticks. (**G**) ASP3026 triggered conformational changes to the important ATP recognition residues Arg330 and His338. ASP3026, Arg330 and His338 are depicted as sticks.

this minor change significantly reduced the ability of NVP-TAE684 to bind *Pf*LysRS (Figure 6B). In the *Pf*LysRS–ASP3026 structure, the azine made one H-bond with a co-bound water, and the water further formed H-bond interactions with the main chain of residues Asp558 and Arg559, capping the adjacent α-helix (Supplementary Figure S10A). The phenylchloride substitution of this azine will cause the loss of these H-bond interactions and may also clash with the Arg559 (Supplementary Figure S10B). As a result, NVP-TAE684 increased the Tm of *Pf*LysRS by 2.92°C in the presence of L-lysine and 1.78°C without L-lysine (Supplementary Figure S10C,D). Consistently, NVP-TAE684 inhibited *Pf*LysRS with an IC_{50} of greater than 50 μM in the ATP hydrolysis assay (Supplementary Figure S10E). In addition, changes to the sulfonylphenyl group and the methoxylphenyl group further decreased the potency. The substitution of the isopropyl in compounds Brigatinib and ALK-IN-1 reduce the interaction with Gly556 (Figure 4C). Finally, changing the methoxyl into an isopropanoxyl group created a clash with Glu332 (Figures 4C

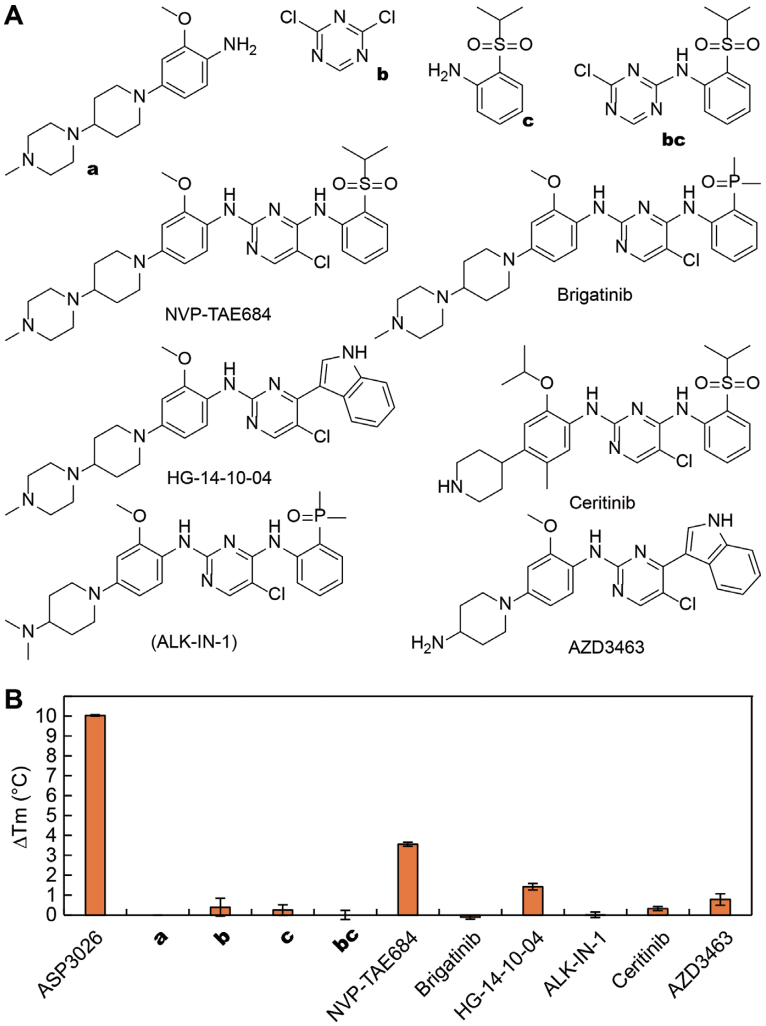

Figure 6. Structure-Activity Profile of ASP3026 for Binding of *Pf*LysRS. (**A**) The chemical structures of compound ASP3026 substructures and analogs. (**B**) Diagram of the ΔTms of *Pf*LysRS in the presence of ASP3026 substructures or analogs without L-lysine. Error bars represent SD of four technical replicates.

and 5E). Together, these results indicate that the interaction of ASP3026 with *Pf*LysRS exhibits a strong structural specificity.

DISCUSSION

In this study, we identified that the clinical trial antitumor drug ASP3026 is a potent *Pf*LysRS inhibitor. It showed significant inhibition of blood-stage *P. falciparum* growth. Revealed by a high-resolution crystal structure, ASP3026 competes with substrate ATP for *Pf*LysRS binding. It also potentially blocks the 3′end of tRNA to enter the active site of *Pf*LysRS. However, it does not interfere with the binding of L-lysine nor show any synergistic binding effect with L-lysine. These characteristics are not observed in previously reported LysRS inhibitors.

It is exciting that the newly finished phase I clinical trial have demonstrated that ASP3026 exhibits very good oral absorption and ideal metabolic stability with a median half-life of 35 h (range, 22–85 h). In addition, the compound is highly tolerable, and the mean of the peak plasma concentration could reach greater than 2.6 μM (1600 ng·ml^{-1}) (27). Therefore, ASP3026 already meets several key requirements for an antimalarial agent. Although it is less feasible to use ASP3026 directly as an antimalarial drug, it provides a promising chemical scaffold with good druggability for further development of antimalarials.

The discovery that ASP3026 is a dual inhibitor for aaRS and kinase is surprising but also inherently plausible. AaRSs and kinases are both enzymes that use ATP as substrates. For the recognition and binding of ATP, their active sites must share certain similarities. Consequently, among all drugs, ATP-competitive kinase inhibitors should have an increased chance of binding to the active site of aaRSs.

AaRSs are attractive targets for drug development for treating infectious diseases, parasitic diseases, and tumors (6–11). However, to date, only three aaRS inhibitors have been approved for use in humans or animals: the isoleucyl-tRNA synthetase (IleRS) inhibitor mupirocin (6,42), prolyl-tRNA synthetase (ProRS) inhibitor halofuginone (10), and leucyl-tRNA synthetase (LeuRS) inhibitor AN2690 (7). One loose explanation for the difficulty of developing

druggable aaRS inhibitors was that the enzymatic pockets of aaRSs have evolved to bind highly polar substrate molecules (amino acids, ATP, or tRNAs); thus, the inhibitors of aaRSs are often too polar to exhibit good druggability. Interestingly, we observed that in the *Pf*LysRS-ASP3026 structure, residues involved in polar interactions with substrates, such as Glu332 and Glu500, could change conformations to form hydrophobic interactions with inhibitors through their aliphatic chains (Figure 5E,F). On the other side, there have been ∼50 approved drugs and >175 oral effective inhibitors in clinical trials targeting protein kinases that share the same substrate, ATP (43). The current research and development of aaRS-inhibiting drugs lag behind that of kinase-targeting drugs (43,44). This study highlights a promising strategy to develop aaRS-targeting drugs by repurposing and modifying compounds from the relatively well-developed kinase inhibitor pool.

DATA AVAILABILITY

Atomic coordinates and structure factors for the reported crystal structure have been deposited with the Protein Data bank under accession number 7BT5.

SUPPLEMENTARY DATA

Supplementary Data are available at NAR Online.

ACKNOWLEDGEMENTS

We thank Dr Dapeng Zhu for his helpful discussion. And we gratefully acknowledge help from staffs of beamline 17U1 at Shanghai Synchrotron Radiation Facility.

FUNDING

National Natural Science Foundation of China [21778064, 21977107, 21778067, 21977108, 31571345]; Strategic Priority Research Program of the Chinese Academy of Sciences [XDB20000000]; Center for Excellence in Molecular Synthesis [FZHCZY020600]; State Key Laboratory of Bioorganic and Natural Products Chemistry; 1000-talent young investigator award; 100-talent program of the Chinese Academy of Sciences; National Key R&D Program of China [2018YFA0507300]. Funding for open access charge: Strategic Priority Research Program of the Chinese Academy of Sciences [XDB20000000].
Conflict of interest statement. None declared.

REFERENCES

1. World Health Organization (ed) (2019) In: *World Malaria Report*. World Health Organization, Geneva.
2. Bhatt,S., Weiss,D.J., Cameron,E., Bisanzio,D., Mappin,B., Dalrymple,U., Battle,K., Moyes,C.L., Henry,A., Eckhoff,P.A. *et al.* (2015) The effect of malaria control on Plasmodium falciparum in Africa between 2000 and 2015. *Nature*, **526**, 207–211.
3. Cui,L., Yan,G., Sattabongkot,J., Cao,Y., Chen,B., Chen,X., Fan,Q., Fang,Q., Jongwutiwes,S., Parker,D. *et al.* (2012) Malaria in the Greater Mekong Subregion: heterogeneity and complexity. *Acta Trop.*, **121**, 227–239.
4. Ibba,M. and Soll,D. (2000) Aminoacyl-tRNA synthesis. *Annu. Rev. Biochem.*, **69**, 617–650.
5. Carter,C.W. Jr (1993) Cognition, mechanism, and evolutionary relationships in aminoacyl-tRNA synthetases. *Annu. Rev. Biochem.*, **62**, 715–748.
6. Silvian,L.F., Wang,J. and Steitz,T.A. (1999) Insights into editing from an ile-tRNA synthetase structure with tRNAile and mupirocin. *Science*, **285**, 1074–1077.
7. Rock,F.L., Mao,W., Yaremchuk,A., Tukalo,M., Crepin,T., Zhou,H., Zhang,Y.K., Hernandez,V., Akama,T. *et al.* (2007) An antifungal agent inhibits an aminoacyl-tRNA synthetase by trapping tRNA in the editing site. *Science*, **316**, 1759–1761.
8. Sundrud,M.S., Koralov,S.B., Feuerer,M., Calado,D.P., Kozhaya,A.E., Rhule-Smith,A., Lefebvre,R.E., Unutmaz,D., Mazitschek,R., Waldner,H. *et al.* (2009) Halofuginone inhibits TH17 cell differentiation by activating the amino acid starvation response. *Science*, **324**, 1334–1338.
9. Gadakh,B. and Van Aerschot,A. (2012) Aminoacyl-tRNA synthetase inhibitors as antimicrobial agents: a patent review from 2006 till present. *Expert Opin. Ther. Pat.*, **22**, 1453–1465.
10. Zhou,H., Sun,L., Yang,X.L. and Schimmel,P. (2013) ATP-directed capture of bioactive herbal-based medicine on human tRNA synthetase. *Nature*, **494**, 121–124.
11. Kim,D.G., Lee,J.Y., Kwon,N.H., Fang,P., Zhang,Q., Wang,J., Young,N.L., Guo,M., Cho,H.Y., Mushtaq,A.U. *et al.* (2014) Chemical inhibition of prometastatic lysyl-tRNA synthetase-laminin receptor interaction. *Nat. Chem. Biol.*, **10**, 29–34.
12. Bhatt,T.K., Kapil,C., Khan,S., Jairajpuri,M.A., Sharma,V., Santoni,D., Silvestrini,F., Pizzi,E. and Sharma,A. (2009) A genomic glimpse of aminoacyl-tRNA synthetases in malaria parasite Plasmodium falciparum. *BMC Genomics*, **10**, 644.
13. Khan,S. (2016) Recent advances in the biology and drug targeting of malaria parasite aminoacyl-tRNA synthetases. *Malar. J.*, **15**, 203.
14. Ge,H. (2016) In: *The Handbook of Prescriptions for Emergencies (In Chinese: Zhou Hou Bei Ji Fang)*. Chinese Medicine Press.
15. Takaya,Y., Tasaka,H., Chiba,T., Uwai,K., Tanitsu,M., Kim,H.S., Wataya,Y., Miura,M., Takeshita,M. and Oshima,Y. (1999) New type of febrifugine analogues, bearing a quinolizidine moiety, show potent antimalarial activity against Plasmodium malaria parasite. *J. Med. Chem.*, **42**, 3163–3166.
16. Herman,J.D., Pepper,L.R., Cortese,J.F., Estiu,G., Galinsky,K., Zuzarte-Luis,V., Derbyshire,E.R., Ribacke,U., Lukens,A.K., Santos,S.A. *et al.* (2015) The cytoplasmic prolyl-tRNA synthetase of the malaria parasite is a dual-stage target of febrifugine and its analogs. *Sci. Transl. Med.*, **7**, 288ra277.
17. Otoguro,K., Ui,H., Ishiyama,A., Kobayashi,M., Togashi,H., Takahashi,Y., Masuma,R., Tanaka,H., Tomoda,H., Yamada,H. *et al.* (2003) In vitro and in vivo antimalarial activities of a non-glycosidic 18-membered macrolide antibiotic, borrelidin, against drug-resistant strains of Plasmodia. *J. Antibiot.*, **56**, 727–729.
18. Fang,P., Yu,X., Jeong,S.J., Mirando,A., Chen,K., Chen,X., Kim,S., Francklyn,C.S. and Guo,M. (2015) Structural basis for full-spectrum inhibition of translational functions on a tRNA synthetase. *Nat. Commun.*, **6**, 6402.
19. Novoa,E.M., Camacho,N., Tor,A., Wilkinson,B., Moss,S., Marin-Garcia,P., Azcarate,I.G., Bautista,J.M., Mirando,A.C., Francklyn,C.S. *et al.* (2014) Analogs of natural aminoacyl-tRNA synthetase inhibitors clear malaria in vivo. *Proc. Natl. Acad. Sci. U.S.A.*, **111**, E5508–5517.
20. Hoepfner,D., McNamara,C.W., Lim,C.S., Studer,C., Riedl,R., Aust,T., McCormack,S.L., Plouffe,D.M., Meister,S., Schuierer,S. *et al.* (2012) Selective and specific inhibition of the plasmodium falciparum lysyl-tRNA synthetase by the fungal secondary metabolite cladosporin. *Cell Host Microbe*, **11**, 654–663.
21. Baragana,B., Forte,B., Choi,R., Nakazawa Hewitt,S., Bueren-Calabuig,J.A., Pisco,J.P., Peet,C., Dranow,D.M., Robinson,D.A., Jansen,C. *et al.* (2019) Lysyl-tRNA synthetase as a drug target in malaria and cryptosporidiosis. *Proc. Natl. Acad. Sci. U.S.A.*, **116**, 7015–7020.
22. Fang,P., Han,H., Wang,J., Chen,K., Chen,X. and Guo,M. (2015) Structural basis for specific inhibition of tRNA synthetase by an ATP competitive inhibitor. *Chem. Biol.*, **22**, 734–744.
23. Chhibber-Goel,J. and Sharma,A. (2019) Side chain rotameric changes and backbone dynamics enable specific cladosporin binding in Plasmodium falciparum lysyl-tRNA synthetase. *Proteins*, **87**, 730–737.

24. Das,P., Babbar,P., Malhotra,N., Sharma,M., Jachak,G.R., Gonnade,R.G., Shanmugam,D., Harlos,K., Yogavel,M., Sharma,A. *et al.* (2018) Specific stereoisomeric conformations determine the drug potency of cladosporin scaffold against malarial parasite. *J. Med. Chem.*, **61**, 5664–5678.
25. Rusch,M., Thevenon,A., Hoepfner,D., Aust,T., Studer,C., Patoor,M., Rollin,P., Livendahl,M., Ranieri,B., Schmitt,E. *et al.* (2019) Design and synthesis of metabolically stable tRNA synthetase inhibitors derived from cladosporin. *Chembiochem.*, **20**, 644–649.
26. Fredenhagen,A., Schroer,K., Schroder,H., Hoepfner,D., Ligibel,M., Porchet Zemp,L., Radoch,C., Freund,E. and Meishammer,A. (2019) Cladosporin derivatives obtained by biotransformation provide guidance for the focused derivatization of this antimalarial lead compound. *Chembiochem.*, **20**, 650–654.
27. Li,T., LoRusso,P., Maitland,M.L., Ou,S.H., Bahceci,E., Ball,H.A., Park,J.W., Yuen,G. and Tolcher,A. (2016) First-in-human, open-label dose-escalation and dose-expansion study of the safety, pharmacokinetics, and antitumor effects of an oral ALK inhibitor ASP3026 in patients with advanced solid tumors. *J. Hematol. Oncol.*, **9**, 23.
28. Al Mamun Bhuyan,A., Bissinger,R., Cao,H. and Lang,F. (2017) Inhibition of erythrocyte cell membrane scrambling by ASP3026. *Cell. Physiol. Biochem.*, **43**, 507–517.
29. Bradford,M.M. (1976) A rapid and sensitive method for the quantitation of microgram quantities of protein utilizing the principle of protein-dye binding. *Anal. Biochem.*, **72**, 248–254.
30. Pantoliano,M.W., Petrella,E.C., Kwasnoski,J.D., Lobanov,V.S., Myslik,J., Graf,E., Carver,T., Asel,E., Springer,B.A., Lane,P. *et al.* (2001) High-density miniaturized thermal shift assays as a general strategy for drug discovery. *J. Biomol. Screen.*, **6**, 429–440.
31. Wang,Q.-S., Zhang,K.-H., Cui,Y., Wang,Z.-J., Pan,Q.-Y., Liu,K., Sun,B., Zhou,H., Li,M.-J., Xu,Q. *et al.* (2018) Upgrade of macromolecular crystallography beamline BL17U1 at SSRF. *Nuclear Sci. Techn.*, **29**, 68.
32. Winter,G., Lobley,C.M. and Prince,S.M. (2013) Decision making in xia2. *Acta Crystallogr. D Biol. Crystallogr.*, **69**, 1260–1273.
33. Vagin,A. and Teplyakov,A. (2010) Molecular replacement with MOLREP. *Acta Crystallogr. D Biol. Crystallogr.*, **66**, 22–25.
34. Emsley,P., Lohkamp,B., Scott,W.G. and Cowtan,K. (2010) Features and development of Coot. *Acta Crystallogr. D Biol. Crystallogr.*, **66**, 486–501.
35. Adams,P.D., Afonine,P.V., Bunkoczi,G., Chen,V.B., Davis,I.W., Echols,N., Headd,J.J., Hung,L.W., Kapral,G.J., Grosse-Kunstleve,R.W. *et al.* (2010) PHENIX: a comprehensive Python-based system for macromolecular structure solution. *Acta Crystallogr. D Biol. Crystallogr.*, **66**, 213–221.
36. Khan,S., Sharma,A., Belrhali,H., Yogavel,M. and Sharma,A. (2014) Structural basis of malaria parasite lysyl-tRNA synthetase inhibition by cladosporin. *J. Struct. Funct. Genomics*, **15**, 63–71.
37. Zhou,J., Zheng,L., Hei,Z., Li,W., Wang,J., Yu,B. and Fang,P. (2020) Atomic resolution analyses of isocoumarin derivatives for inhibition of lysyl-tRNA synthetase. *ACS Chem. Biol.*, **15**, 1016–1025.
38. Iikubo,K., Kondoh,Y., Shimada,I., Matsuya,T., Mori,K., Ueno,Y. and Okada,M. (2018) Discovery of N-{2-Methoxy-4-[4-(4-methylpiperazin-1-yl)piperidin-1-yl]phenyl}-N'-[2-(propane-2-sulfonyl)phenyl]-1,3,5-triazine-2,4-diamine (ASP3026), a Potent and Selective Anaplastic Lymphoma Kinase (ALK) Inhibitor. *Chem. Pharm. Bull.*, **66**, 251–262.
39. Karimi,A., Navidbakhsh,M., Motevalli Haghi,A. and Faghihi,S. (2013) An innovative shape equation to quantify the morphological characteristics of parasitized red blood cells by Plasmodium falciparum and Plasmodium vivax. *Proc. Inst. Mech. Eng. H*, **227**, 428–437.
40. Smilkstein,M., Sriwilaijaroen,N., Kelly,J.X., Wilairat,P. and Riscoe,M. (2004) Simple and inexpensive fluorescence-based technique for high-throughput antimalarial drug screening. *Antimicrob. Agents Chemother.*, **48**, 1803–1806.
41. Khan,S., Garg,A., Camacho,N., Van Rooyen,J., Kumar Pole,A., Belrhali,H., Ribas de Pouplana,L., Sharma,V. and Sharma,A. (2013) Structural analysis of malaria-parasite lysyl-tRNA synthetase provides a platform for drug development. *Acta Crystallogr. D Biol. Crystallogr.*, **69**, 785–795.
42. Hughes,J. and Mellows,G. (1980) Interaction of pseudomonic acid A with Escherichia coli B isoleucyl-tRNA synthetase. *Biochem. J.*, **191**, 209–219.
43. Roskoski,R. Jr (2019) Properties of FDA-approved small molecule protein kinase inhibitors. *Pharmacol. Res.*, **144**, 19–50.
44. Wu,P., Nielsen,T.E. and Clausen,M.H. (2015) FDA-approved small-molecule kinase inhibitors. *Trends Pharmacol. Sci.*, **36**, 422–439.